ACS OMEGA

Open Access

http://pubs.acs.org/journal/acsodf

Article

Effective Removal of Carcinogenic Azo Dye from Water Using *Zea mays*-Derived Mesoporous Activated Carbon

Fathy M. Mohamed, Mohamed R. El-Aassar,* Omar M. Ibrahim, Aya Elsayed, Manal F. Alrakshy, Mohamed Abdel Rafea, and Kawthar A. Omran*

Cite This: *ACS Omega* 2024, 9, 13086−13099

Read Online

ACCESS | Metrics & More | Article Recommendations

ABSTRACT: Addressing industrial wastewater treatment challenges and removing hazardous organic pollutants, such as carcinogenic methyl orange (MO) and azo dyes, is a pressing concern. This study explores the use of the *Zea mays* envelope, an agricultural waste product, to produce *Z. mays* activated carbon (ZMAC) through the chemical activation of maize envelopes with phosphoric acid. Various analytical techniques, including FTIR, XRD, TGA, DSC, and SEM, characterize ZMAC. Results show that ZMAC exhibits an impressive monolayer adsorption capacity of 66.2 mg/g for MO. The Langmuir isotherm model fits the experimental data well, indicating monolayer coverage of the MO on the ZMAC surface. The pH-sensitive adsorption process demonstrates an optimal removal efficiency at pH 4. ZMAC follows the pseudo-second-order kinetic model, and diffusion rate constant analysis identifies three consecutive stages in the adsorption process. Moreover, the uptake of MO ions by ZMAC is identified as an exothermic and spontaneous process. Reusability tests demonstrate efficient regeneration of ZMAC up to five times with 1 mL of 2 M HNO_3 in each cycle, without sorbent mass loss. Thermodynamic analysis shows an increase in the uptake capacity from 66.2 to 73.2 mg/g with temperature elevation. This study offers practical solutions for industrial wastewater treatment challenges, providing an environmentally sustainable and effective approach to mitigate the risks associated with hazardous organic pollutants.

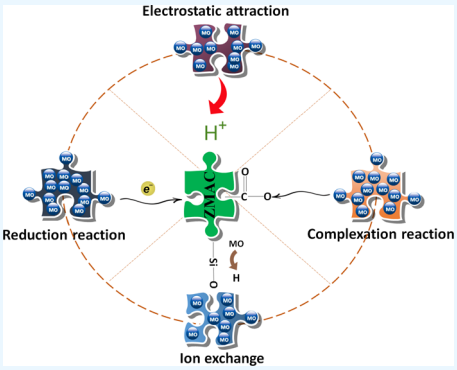

1. INTRODUCTION

The scientific community is advocating for the utilization of agricultural waste recycling and increased investment in the mitigation of environmental pollutants. This call extends to addressing a spectrum of contaminants, including both organic compounds and heavy metals. It is particularly crucial for developing nations contending with the compounding issue of environmental pollution, which has been further exacerbated by the surge in global population.[1]

There are over 100,000 types of dyes available commercially, with production exceeding one million tons annually. It was estimated that more than 20% of dyes are discharged directly into the environment.[2] Disposal of dyes without pretreatment into the water streams causes intense ecological disturbance and pollution of marine life.[3] Methyl orange (MO) is one of the most recent dyes used in the textile industry.[4] It is also used as a pH indicator for titrations in lab.[5,6] MO make up an abundant class of azodye characterized by the presence of unsaturated groups (chromophores) such as −C═C−, −N═N−, and −C≡N−, which are responsible for the dye colors, and of functional groups responsible for their fixation to fibers, for example, $-NH_2$, and $-SO_3H$.[7] Although most dyes have low toxicity, their components and breakdown products can be more toxic. In addition, improperly discharged industrial dyes pose a danger to human health. To overcome this problem, much attention has been focused on the effective treatment of dyes discharged from the dying industries. The chemical structure of MO is shown in Scheme 1.

Scheme 1. Chemical Structural of Methyl Orange

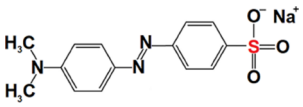

According to The Environment (Protection) Rules, New Delhi, 1986, the permissible limits of organic materials in surface water expressed as COD and BOD are 250 and 30 mg/L, respectively.

The escalation of the ecological burden is a direct consequence of inadequate solid waste and agro-residue

Received: November 30, 2023
Revised: February 14, 2024
Accepted: February 22, 2024
Published: March 4, 2024

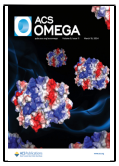

Table 1. Factors Affecting of MO onto ZMAC

factors	conditions						
pH	2	3	4	5	7	8	9
dose (mg)	2	4	6	8	10	12	15
contact time (min.)	15	30	60	90	120	180	
temperature (k)	298	303	308	313	318		
agitation forth (RPM)	50	100	150	200	250		
adsorbate concentration (mg/L)	5	15	20	30	40		

management.[8,9] The presence of heavy metals in conventional water sources poses a significant health risk to humans, leading to detrimental effects on the nervous system, liver fibrosis, kidney failure, increased bone fragility, interference with crucial enzyme functional groups, and the onset of various chronic disorders.[10] Various agro-residue utilization systems have been explored, including strategies such as straw incorporation into agricultural fields, straw-based power generation, anaerobic decomposition for biogas production, and straw gasification to yield biogas.[11]

Surface water, groundwater, and industrial wastewater are subject to contamination through human activities, with the treatment of wastewater containing a diverse range of organic and low-charge substances being a current challenge. The production of activated carbon (AC) offers an efficient means of harnessing renewable energy from agricultural residues while simultaneously mitigating environmental pollution. AC derived from renewable sources such as corn stalks, rice husks, and bagasse exhibits substantial specific surface areas and well-developed pore structures.[12] Expanding the surface area and enhancing the pore characteristics of agricultural residues are key factors in optimizing their efficacy.[12,13]

Agro-residues have demonstrated the capability to remove various organic substances, including methylene blue,[14] aniline,[15] PAHs,[16] norfloxacin,[17] phenol,[18] MO,[19] residue of waste penicillin mycelium,[20] atrazine,[1] toluene,[21] and acid orange 7.[22]

There are many precursors for the removal of MO such as SiO_2 NPs, which recorded the maximum adsorption capacity of 69.40 mg/g.[23] Fabricated Fe-loaded chitosan (Fe-CS) film immobilized onto a glass support also recorded 97.1 (303 K), 102 (313 K), and 205 mg/g (323 K).[24] The adsorption kinetic model of functionalized-CNTs loaded TiO_2 follows a pseudo-second-order with a maximum adsorption capacity of 42.85 mg/g.[25] Coffee waste/methylpyridinium chloride recorded the maximum adsorption capacity of 62.50.[26] Coffee waste/cetyltrimethylammonium ammonium bromide recorded the maximum adsorption capacity of 58.82,[26] and surfactant-modified pineapple leaf recorded the maximum adsorption capacity of 47.62.[27]

The pressing need for effective treatment of industrial wastewater, particularly in the removal of hazardous organic pollutants such as carcinogenic MO and azo dyes, has prompted innovative research in the field. This article introduces the novelty of utilizing ZMAC, derived from agricultural waste (*Zea mays* envelope), for the adsorptive removal of pollutants. The uniqueness of this study lies in the comprehensive exploration of ZMAC's adsorption capabilities, offering a sustainable and efficient solution to address environmental challenges associated with industrial wastewater.

The present study is driven by the following research goals: (1) to investigate the transformation of *Z. mays* husk (ZMAC) into modified *Z. mays* husk ash (ZMAC) through the application of phosphoric acid. (2) To demonstrate the enhanced removal efficiency of the carcinogenic compound, MO was facilitated by the introduction of H_3PO_4. (3) To establish a well-defined batch system for the systematic examination of experimental variables. (4) To employ a comprehensive set of kinetic, thermodynamic, and isotherm models to analyze and interpret the obtained data.

2. MATERIALS AND METHODS

2.1. *Z. mays* Husk. *Z. mays* husk (ZMH) was collected from beni-Suef governorate as solid waste of agro-residues.

2.2. Chemicals. H_3PO_4 laboratory grade in powder form is used for preparing an aqueous solution of H_3PO_4 of specific concentration. For initial pH adaptations, regeneration investigations, and other applications, Al-Naser Company provided H_2SO_4 and NaOH.

2.3. Preparation of ZMAC. The representative sample (20 g) of *Z. mays* husk is immersed in phosphoric acid for 24 h, washing with distilled water until neutral pH. After the product has been dried for 2 h at 105 °C, the fractions (4 g) are retrieved and put in the desiccator after being washed again with ultrapure water. The dried *Z. mays* activated carbon (ZMAC) sample was packaged under the ZMAC nameplate and ground below 100 m.

2.4. Material Characterization. ZMAC was characterized by X-ray diffraction model Philips APD-3720 diffractometry, DSC (TA Instruments Q2000 DSC), Raman spectra (Bruker, Senterra II, Germany), TGA (Q500 equipment thermo gravimetric analyzer), scanning electron microscopy (JSM-6700F, JEOL, Japan), and SBET. The nitrogen adsorption-desorption isotherms at 77 K were measured using a NOVA 4200e (Quantachrome Instruments, USA). The specific surface area and pore size were then analyzed using the Brunauer-Emmett-Teller (BET) equation. Additionally, the pore size distributions were estimated using the Barrett-Joyner-Halenda (BJH) technique based on the isothermic adsorption branch.

2.5. Batch Experiments. To identify the optimal adsorption conditions, a concentration range of 5−60 mg/L of MO was used. This concentration range was used to study the following conditions, including the adsorbent dose (ranging from 2 to 15 mg/L), solution pH (adjusted from 2 to 9 using HCl and NaOH), agitation rate (varying from 50 to 250 rpm), and temperature (maintained between 298 and 318 K) at different residence times (spanning from 5 to 180 min) (Table 1).

Twenty milligrams amount of the composite was mixed with 50 mL of the MO solution for 120 min at a constant temperature of 25 °C. The mixture of adsorbate and adsorbent was separated by centrifugation. The remaining concentration of MO was measured with a spectrophotometer at 468 nm.[28]

https://doi.org/10.1021/acsomega.3c09494
ACS Omega 2024, 9, 13086−13099

Table 2. Physical Characteristics of ZMAC from Nitrogen Adsorption Isotherms

sample	surface area (m^2/ g) (SBET)	pore volume (cm^3/ g) (Vt)	average pore diameter (nm)
ZMAC	133.225	0.126513	2.046

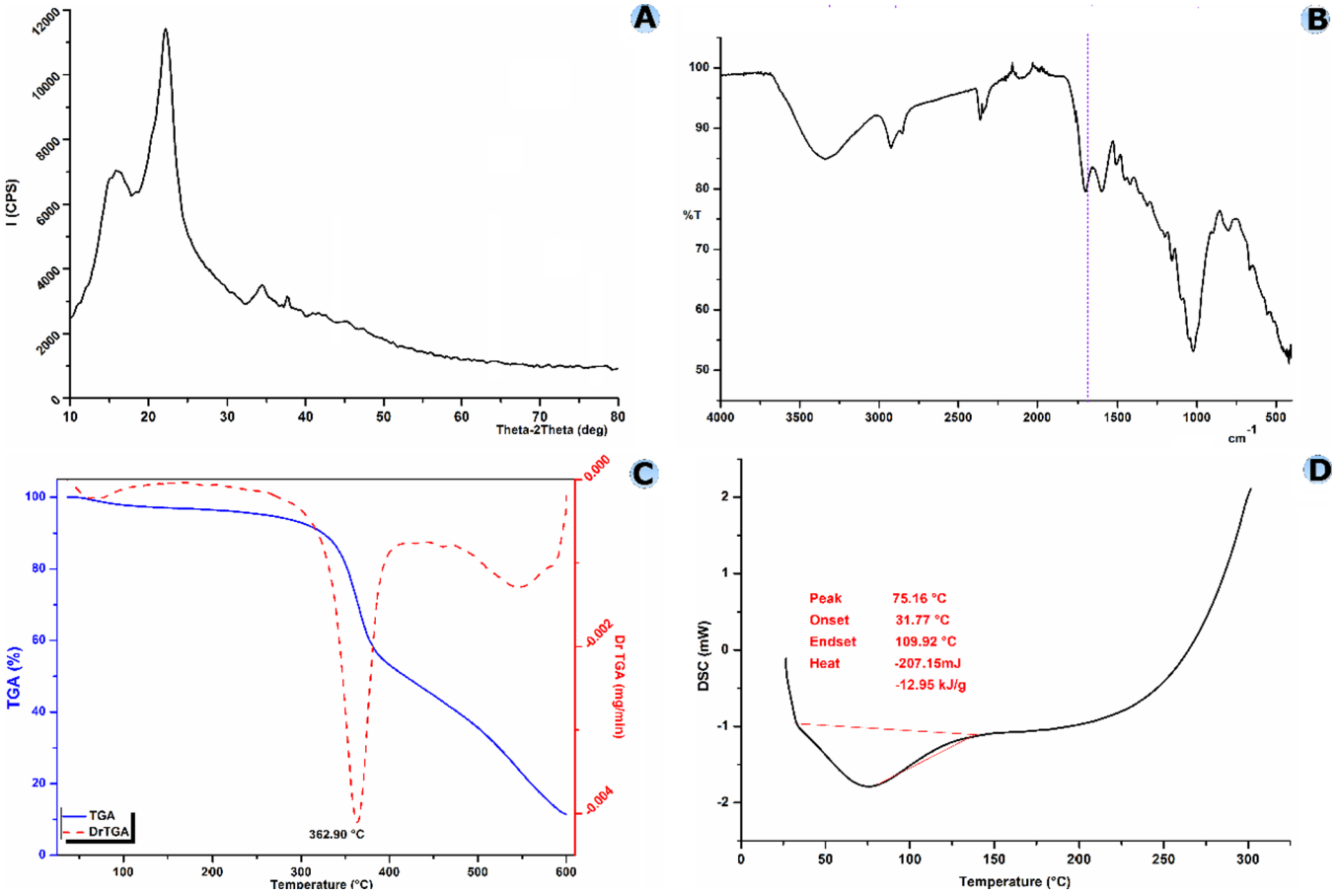

Figure 1. Characterization of ZMAC: XRD (A), ATR-FTIR spectra (B), TGA (C), and DSC (D).

We performed triplicate samples to estimate the cleansing efficacy (R percent) and adsorption capacity (qe, mg/g).[29]

Each sample underwent a triple evaluation, and the resultant average value was documented. The removal percentage and adsorption capacity in milligrams per gram were determined by using eqs 1 and 2.

For the point of zero charge (pHPZC), 10 mg of ZMAC was added to a 0.1 M NaCl solution. The initial pH (pHi) was measured, and then the mixture was agitated at 200 rpm for 60 min, after 24 h, and the final pH (pHf) was measured. To establish pHi, pHPZC was obtained by plotting difference between pHf and pHi against pH values.[30]

$$\mathrm{R}\% = \frac{C_0 - C_e}{C_0} \times 100 \tag{1}$$

$$q_e = \frac{(C_0 - C_e)V}{W} \tag{2}$$

where C_0 and C_e are the MO initial and equilibrium concentrations (mg/L); respectively. V is the MO volume (L) and W is the adsorbent weight (g).

2.6. Kinetics, Isotherms, and Thermodynamics. We used pseudo-first-order, pseudo-second-order, Elovich, and intraparticle-diffusion models:[31,32]

$$\ln(q_e - q_t) = \ln q_e - k_1 t \tag{3}$$

$$\frac{t}{q_t} = \frac{1}{k_2 q_e^2} + \frac{t}{q_e} \tag{4}$$

$$q_t = \beta \ln(\alpha\beta) + \beta \ln t \tag{5}$$

$$q_t = K_p t^{0.5} + C \tag{6}$$

The constants associated with the rate parameters pertain to the pseudo-first- and second-order models, and they are denoted by the values k_1 (in units of min^{-1}) and k_2 (in units of g/g·min). The adsorption rate, measured in g/g·min, corresponds to the number of potential active sites in the system (g/g). Additionally, K_p (in units of g/g·min) and C are representative of the rate constant and the intercept, respectively. F, defined as q_t/q_e, signifies the fraction of adsorbed solute at time t.

The three isotherms—Langmuir,[33] Freundlich,[34] and Tempkin and Pyzhev[35]—were used in the manner depicted in Table 3. To examine the MO adsorption mechanism onto the ZMAC, each isotherm was put to use. Additionally, kinetic adsorption models like those in Table 4 Lagergren[36] and Ho and McKay[37] were preceded.

https://doi.org/10.1021/acsomega.3c09494
ACS Omega 2024, 9, 13086−13099

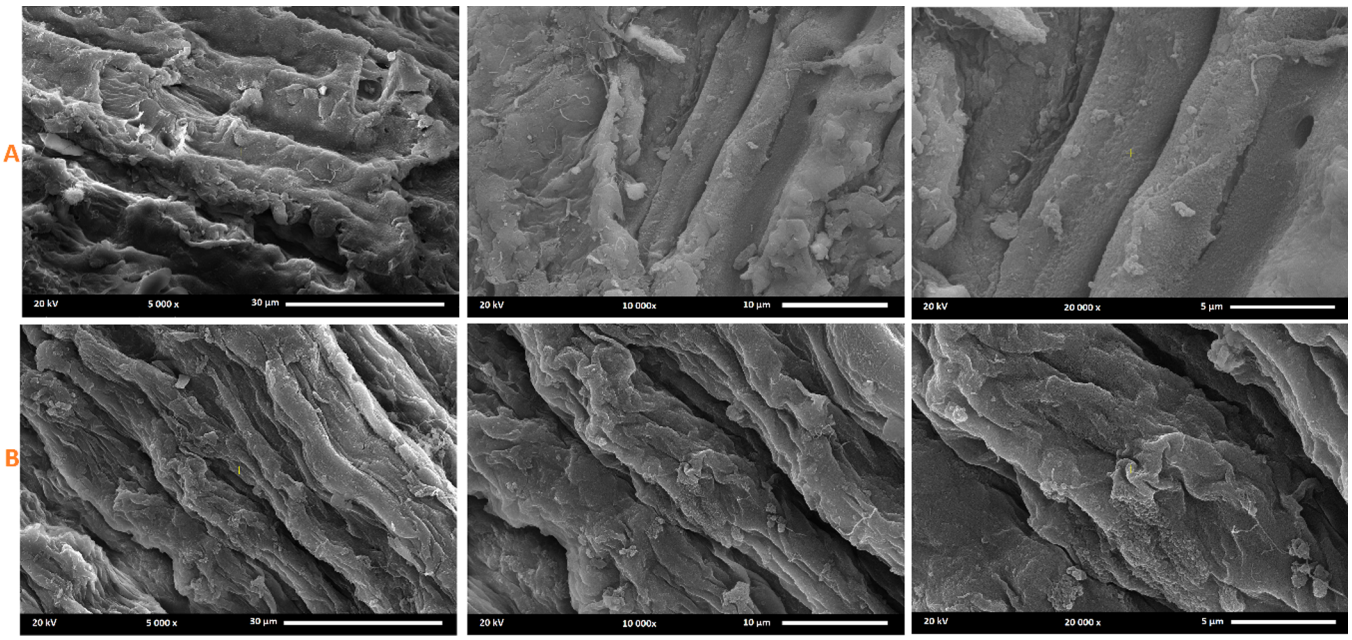

Figure 2. FESEM images at different magnifications of ZMAC (A) before and (B) after MO dye adsorption.

$$\frac{C_e}{q_e} = \frac{1}{q_{max}K_L} + \frac{C_e}{q_{max}} \quad (7)$$

$$\ln q_e = \ln K_F + \frac{1}{n}\ln C_e \quad (8)$$

$$q_e = B_T \ln KT + B_T \ln C_e \quad (9)$$

The saturated adsorption capacity is denoted as qmax (in units of g/g), and the Langmuir isotherm constant is represented as K_L (in units of L/g). The parameter $1/n$ characterizes the adsorption intensity, whereas K_F signifies the adsorption capacity. B stands for adsorption (in units of J/mol), and K_T represents the maximum binding energy (in units of L/g). The dimensionless separation factor, R_L, as defined in eq 10, serves as an indicator of the adsorption favorability:[38]

$$R_L = \frac{1}{1 + K_L C_o} \quad (10)$$

The saturation adsorption capacity is denoted as q_{max} (in units of g/g), and the Langmuir isotherm constant is expressed as K_L (in units of L/g). The parameter $1/n$ signifies the adsorption intensity, while K_F represents the adsorption capacity. The dimensionless separation factor (R_L, see eq 10) can be used to describe the adsorption favorability:[38]

$$\ln K_D = -\frac{\Delta H}{RT} + \frac{\Delta S}{R} \quad (11)$$

$$\Delta G = \Delta H - T\Delta S \quad (12)$$

2.7. Comparative Study for Different Dyes Removal Using ZMAC. A comparison between the applied procedures in this study for dyes removal from a certain industrial wastewater was performed, which uses the removal of different dyes such as crystal violet, methylene blue, and MO. Percentage removal was confirmed by HACK 6000.

2.8. Reusability Test. ZMAC was soaked in 1 M HNO_3 for 2 h, during which time the number of adsorption−desorption cycles was counted.

3. RESULTS AND DISCUSSION

3.1. Characterization of ZMAC. *Z. mays* activated carbon (ZMAC) had a surface area of 133.225 m^2/g. Pore volume in that area was 0.126513 cm^3/g. The average pore size was 2.046 nm. Variable tendency on the pore size is clearly visible in the ZMAC pore size distributions. ZMAC leads to increased pore volume and surface area because of its evident pore distribution in the 0.1−1 nm range and the appearance of a few big pores in the 1−38 nm region, which are compatible with the BET surface area. Average pore sizes for ZMAC have a mostly microporous structure (Table 2).

3.2. Identification of ZMAC. As shown in Figure 1A, the identical diffraction peak was confirmed by X-ray diffraction data from ZMAC; however, it is slightly offset and has a higher intensity of ZMAC, suggesting that volatile components had evaporated. The 26.5° peak indicates an amorphous graphite structure. Another peak formed at 43.9° when the random layer lattice structure of ZMAC was taken into consideration, whereas a faint peak of graphite appeared at 43.8°. The strong peak at 25 degrees and silicon dioxide reflection are connected.[31] The 26.4 diffraction may be due to crystalline carbon in the coal samples.

Figure 1B presents the FTIR spectra of ZMAC. 3315 cm^{-1} may represent the stretching of O−H bonds, while 1740 cm^{-1} and 2952 cm^{-1} represent the asymmetric CH_3 and asymmetric CH stretching modes. Additionally, a set of peaks within the range of 1000−1100 cm^{-1} is observed. The peak at 1098 cm^{-1} may be attributed to the rocking of CH_3 or the wagging of CH_2 modes, and the peak at 1114 cm^{-1} indicates the asymmetric stretching vibrations of Si−O bonds, which are typically found in impurities of aluminosilicate.[39−41] 1280 cm^{-1} may represent the stretching vibrations of C−C and C═C bonds in structures resembling alkenes. The extent of disorder within the graphitic layers of ZMAC is assessed by the similarity in the position of a broad peak, as evidenced in the ZMAC spectra. This observation aligns with findings from prior studies on graphitic materials and supports this characterization.[42] The TGA of the ZMAC sample is shown in Figure

https://doi.org/10.1021/acsomega.3c09494
ACS Omega 2024, 9, 13086−13099

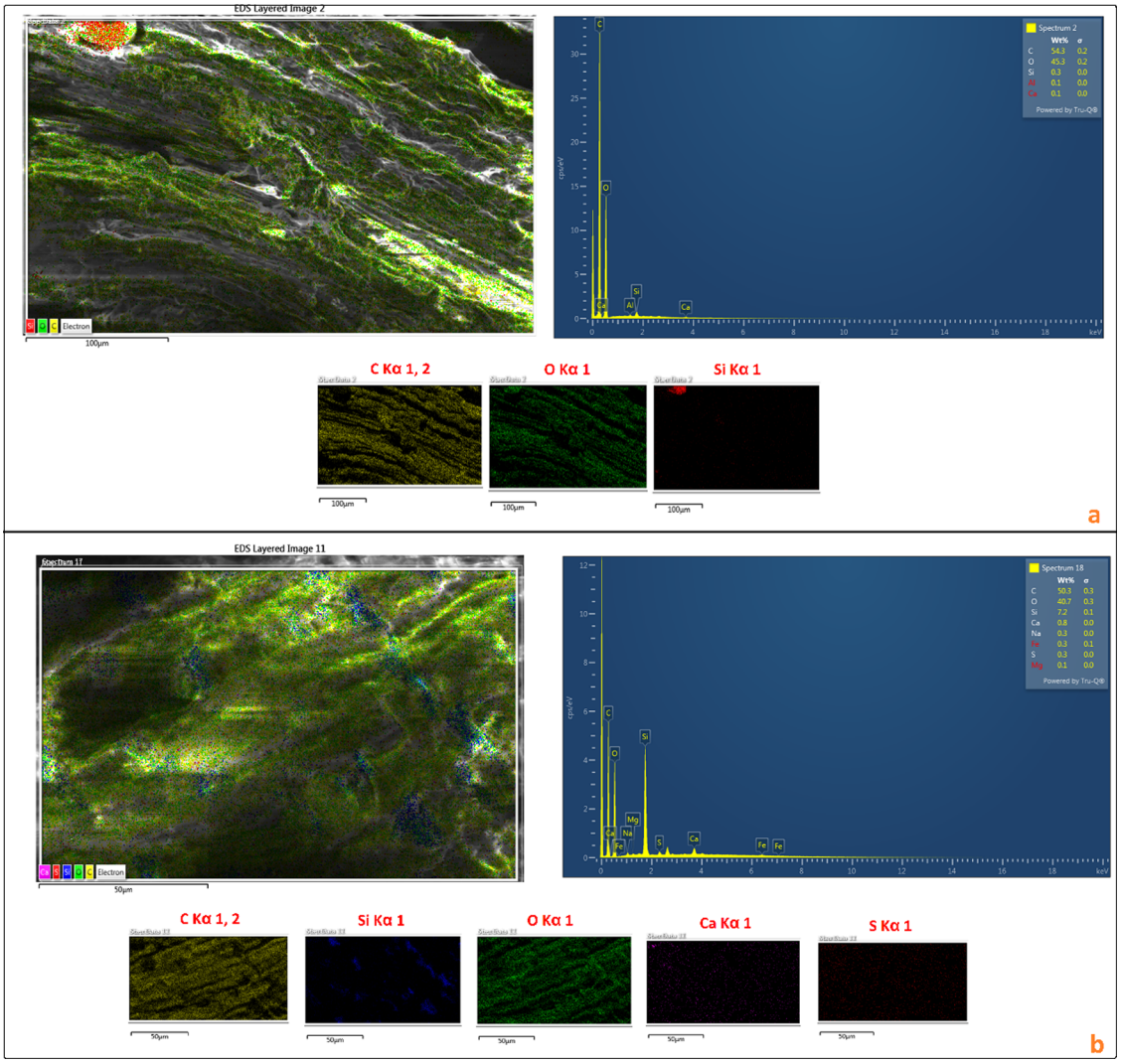

Figure 3. Energy dispersive X-ray (EDX) mapping analysis and elemental analysis of ZMAC. (a) Before MO removal and (b) after MO removing.

1C, indicating a single stage of weight loss at various temperatures. The first was 30% at 350 °C, which may be related to the liberation of volatile organic chemicals.[14,29] The DSC thermogram of ZMAC is shown in Figure 1D, and it shows the loss of volatile materials at 350 °C. The DSC thermogram exhibited endothermic behavior attributed to the release of organic constituents and volatile gases from ZMAC.

In Figures 2 and 3, the scanning electron microscopy (SEM) images offer a comprehensive understanding of the morphological alterations observed in ZMAC both before (A) and after (B) the adsorption of MO dye. In Figure 2A, the SEM micrographs depict the distinctive porous and flaky characteristics of *Z. mays*-derived mesoporous activated carbon (ZMAC), showcasing evident variations in both grain sizes and shapes. The morphological analysis reveals the agglomeration and delineation of material within ZMAC, featuring small and flaky particles. Additionally, the surface of ZMAC exhibits a smooth texture with irregularities, signifying the presence of diverse porous structures of varying sizes and configurations, as illustrated in Figure 2. The confirmation of hexagonal graphite crystals in the micrographs aligns with the X-ray diffraction (XRD) findings. On the other hand, Figure 3 illustrates the adsorption of MO dye onto ZMAC. Changes in the surface morphology become evident, featuring clustered particles that signify the presence of adsorbed dye molecules. When observed at higher magnifications, the SEM images reveal intricate details of the porous architecture of ZMAC (A) before MO adsorption, while (B) showcases the close interaction between MO dye and the AC surface. This visual representation elucidates the efficacy of ZMAC as an adsorbent, providing microscopic evidence of dye attachment and distribution.

Additionally, Figure 3 presents the results of EDX mapping analysis and elemental analysis for ZMAC before and after MO dye adsorption using a SEM-EDAX image. Before adsorption, irregular morphology with minerals embedded in a carbonaceous substrate was revealed by surface morphology. The EDAX data showed that C, O, and Si for ZMAC (weight percent) were present as important components. ZMAC also revealed both luminous and nonluminous properties. In ZMAC, large particles with a diameter of 10 m were recognized as SiO_2. However, following MO dye adsorption, the EDX spectra exhibited additional peaks associated with elements present in the dye such as sulfur. The EDX mapping analysis provided spatial distribution information, confirming the presence of these additional elements on the ZMAC surface after the adsorption process. Based on SEM-EDAX analysis, the surface area (133 m^2/g) increased due to an

https://doi.org/10.1021/acsomega.3c09494
ACS Omega 2024, 9, 13086−13099

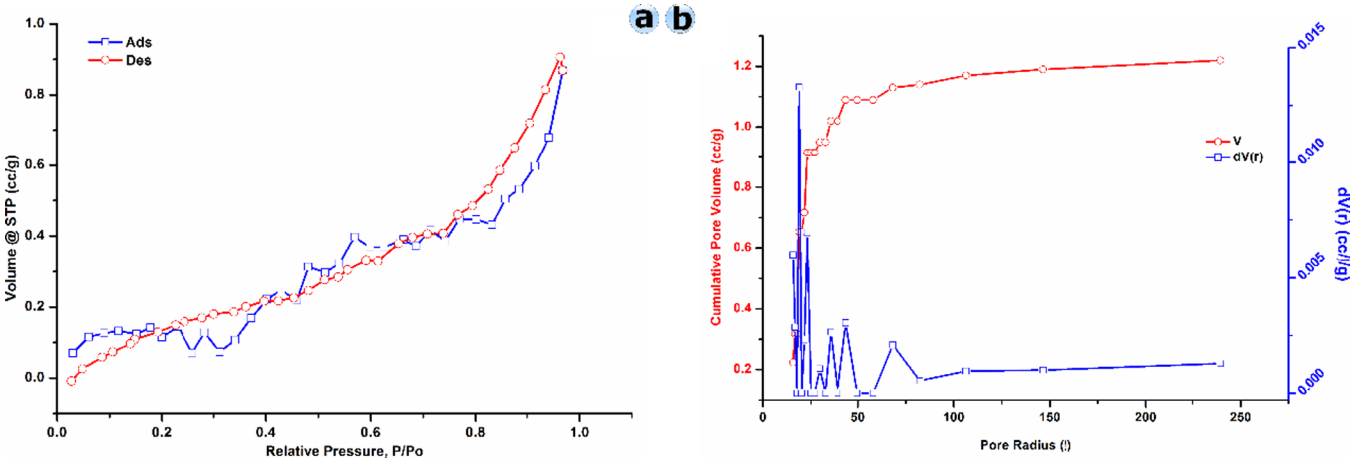

Figure 4. (a) Nitrogen adsorption and desorption isotherms of ZMAC at 77 K and (b) BJH desorption pore size distribution plot of ZMAC.

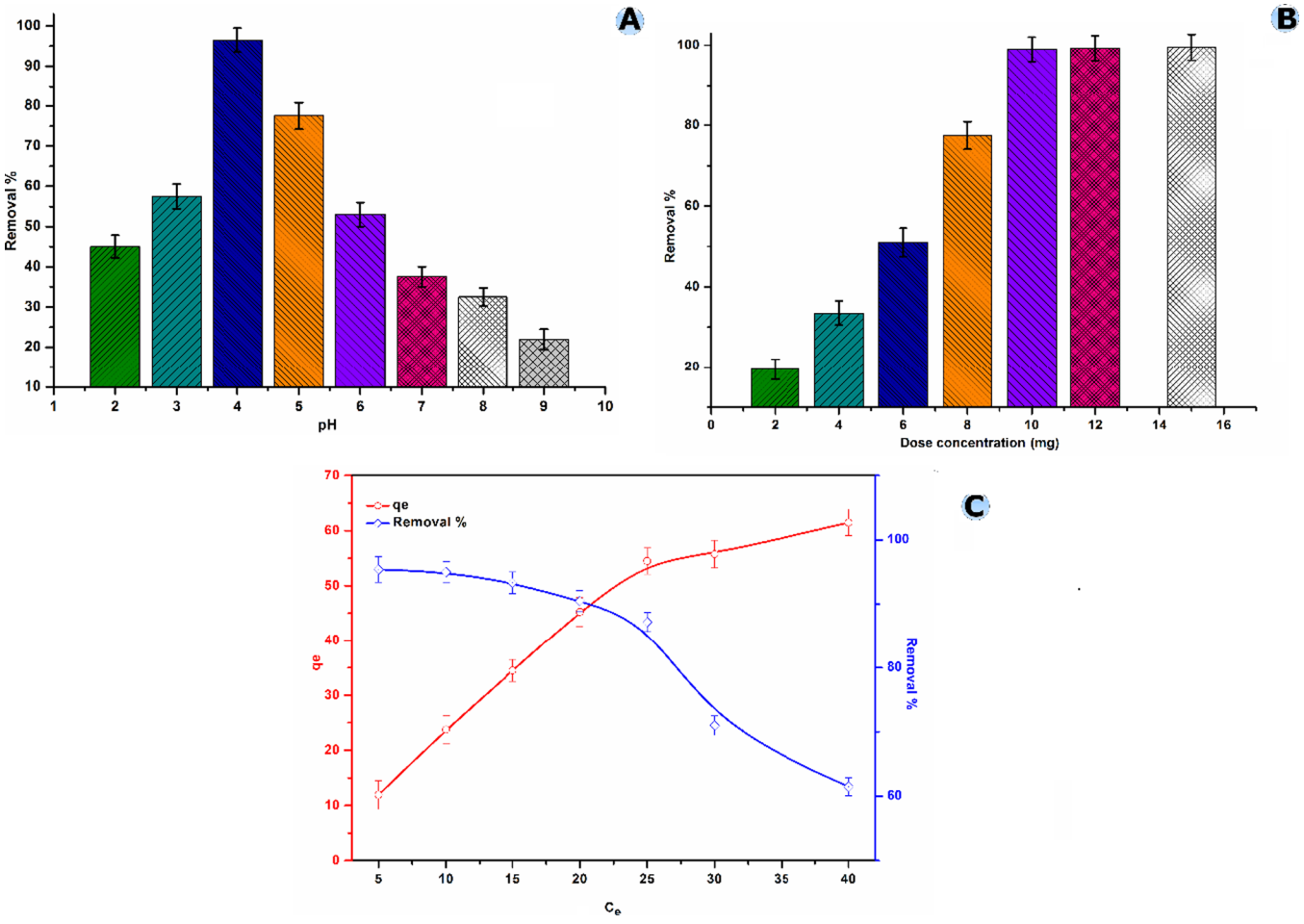

Figure 5. Affecting factors of MO removal: pH (A), dose (B), and initial concentration (C).

increase in cavities.[43] These holes developed after volatile gases including carbon dioxide, carbon monoxide, and hydrogen gases were treated.[43]

Characterization using the BET and BJH models was carried out to further comprehend the alteration effects on the pore structure. The derived ZMAC is classified by IUPAC as being compatible with type I isotherms.[44] In light of this, the resulting ZMAC mostly possesses a mesoporous structure. The microspores within the ZMAC eventually grew from 0.356 to 0.361(cm^3/g), considerably 133 m^2/g increase in the surface area. Anthracite is often neat when shrinking pores between the layers occurred during thermal treatment. As a result, the treatment can significantly widen the pore contents of anthracite. It is obvious from the pore size distributions in Figure 4 that there is a propensity for fluctuation in pore size. A few big pores developed in the region of 2−50 nm, whereas ZMAC (according to the BJH desorption average pore

https://doi.org/10.1021/acsomega.3c09494
ACS Omega 2024, 9, 13086−13099

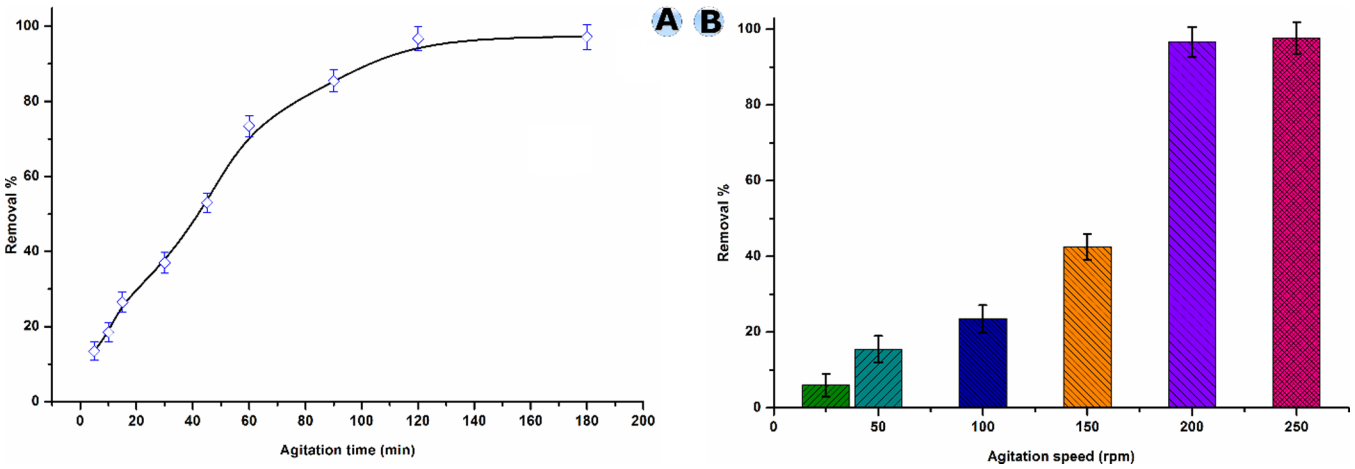

Figure 6. Affecting factors of MO removal: agitation time (A) and agitation speed (B).

diameter) exhibits a noticeable pore distribution in the 5−15 nm range.

3.3. Adsorption Affecting Factors. *3.3.1. pH.* ZMAC's adsorption approach is pH sensitive. Figure 5A illustrates that the MO removal percent (*R* percent) by ZMAC was immense across a wide variety of pH states (3.0−9.0). But only at pH 4.0 did the maximum elimination efficiency eventuate (95%). As a result, pH 4 was ideal to be used for subsequent experiments. MO negative charge was neutralized and adsorbed on the surface of ZMAC due to the protonation process at pH 4, which caused the adsorption capacity to reach its maximum. pH inversely correlates with protonation, leading to reduced adsorption capacity and cleansing percentage.

Figure 5A illustrates the results, which indicate that the sorption of MO increased from pH 2 to 3.0, then marginally increased from pH 3 to 4.0, and then steadily decreased across the remaining pH range from 4.0 to 9.0. The reason for this is that ZMAC is protonated at low pH levels, where H^+ ions create an electrical attraction that is noticeably strong between the ZMAC surface and the MO molecules, resulting in maximal adsorption. Two mechanisms were identified as the cause of the dye's decreased adsorption capacity: the first was the electrostatic attraction between the protonated functional groups of ZMAC and MO, and the second was the chemical interaction between MO and the adsorbents. Because there were more protons accessible at lower pH levels, there was stronger electrostatic interaction between the positively charged functional groups on ZMAC and the negatively charged MO anions.[45] The number of negatively charged sites increased, and the positive charge on the surface dropped as the solution's initial pH rose. Electrostatic repulsion prevented the anionic dye from bonding to the negatively charged ZMAC surface sites. Additionally, the hydroxide ions and dye molecules competed with one another, and an excess of hydroxide ions led to a significant decrease in adsorption.

3.3.2. Adsorbent Mass Effect. Figure 5B illustrates the pattern of MO adsorption by various selected masses (2−15 mg) of the ZMAC. The increase in MO uptake from 19.5 to 99.0% was accompanied by an increase in (ZMAC) mass from 2 to 15 mg. Therefore, 10 mg dose was appropriate for further experimentation. The increase in the percentage of adsorption of MO with the mass of ZMZC is due to the increase in the number of available sites when we increase the quantity of ZMAC. The quantity MO per unit of mass of ZMAC decreased when the mass of the ZMAC was further increased. This phenomenon is due to the fact that an increase in the mass of adsorbent within the limited volume of solution entails an agglomeration of the adsorbent, consequently reducing the intercellular distances. This mass increase leads to the "screen effect", which prevents access to adsorption sites on the adsorbent

3.3.3. Initial Concentration Effect. Figure 5C shows the MO sorption outline at various leading concentrations (5−40 mg/L). The result obtained shows that the elimination percent is inversely proportional to the first concentration of sorbet MO (*R* percent). 100 mg/L of MO was used for all adsorption experiments to validate the attainment of equilibrium.

3.3.4. Agitation Time Effect. Figure 6A illustrates the adsorption of MO by ZMAC over different time intervals ranging from 5 to 180 min. Notably, as the agitation rate increases, it facilitates the diffusion of MO onto the surface of the adsorbent, resulting in rapid MO adsorption within the time span of 5−180 min.[17,46] Consequently, an agitation duration of 120 min was selected as the optimal agitation time and was employed consistently in all adsorption experiments to ensure the attainment of equilibrium.[14,46]

Two stages of adsorption were involved: a quick phase that took 180 min for ZMAC and resulted in an 85.5% removal rate. High absorption like this suggests that ZMAC has a high chemisorption affinity for MO compounds. Up until equilibrium was reached in the second phase, the rate of adsorption drastically decreased. Given that all of the adsorption sites on the surface of the adsorbent materials are available at the beginning of the process, the first phase of adsorption can be justified. The slowing down in the second phase could be attributed to either pore entrances being blocked by the molecules that have already adsorbed, which prevents other adsorbate molecules from reaching sites in the pores, or the incoming ions being repelled by the fixed molecules, which significantly reduces the speed at which approaching molecules can reach empty adsorption sites. Once equilibrium is attained after 120 min, a series of adsorption and desorption processes begin, both happening at the same rate. In terms of desorption, it may be stated that once the dye has filled the sites and one keeps stirring the solution, some dyes may escape through collision with the surface, making room for further molecules to approach.

https://doi.org/10.1021/acsomega.3c09494
ACS Omega 2024, 9, 13086−13099

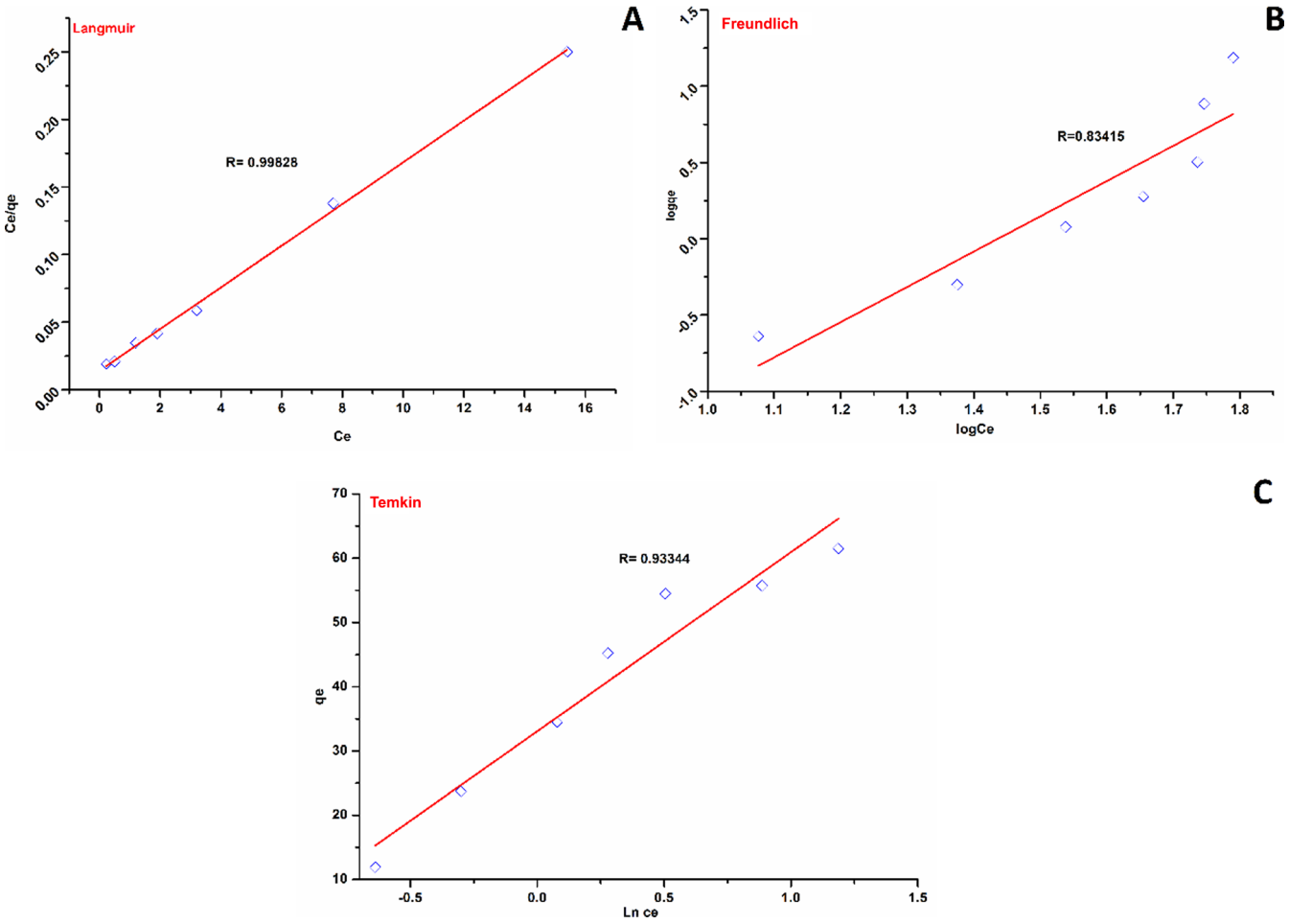

Figure 7. Adsorption isotherm models: (A) Langmuir model, (B) Freundlich model, and (C) Temkin model.

Table 3. Isotherm Constants of MO Adsorption onto ZMAC

	Langmuir				Freundlich			Temkin			
adsorption system	q_e (mg/g)	b (l/mg)	R^2	R_L	k_f	n	R^2	B	A	R^2	b
MO	66.2	1.01	0.998	0.019	0.000478	0.43	0.834	27.86	15.83	0.933	88.9

3.3.5. Agitation Speed. Figure 6B was employed to illustrate the adsorption behavior of MO under different agitation speeds, ranging from 25 to 250 rpm. Notably, the removal percentage of MO exhibited a rapid increase, ranging from 6 to 97.0%, within the agitation speed range of 25−250 rpm. Consequently, an agitation speed of 200 rpm was identified as the optimal agitation speed and was consistently applied in all adsorption investigations to ensure the achievement of equilibrium.

3.4. Adsorption Isotherms. In this study, we elucidated and interpreted the fundamental interaction mechanism between MO ions and ZMAC. This was achieved by employing the linear equations associated with three widely used isotherm models (Figure 7A−C and Table 3). Understanding the interaction between MO and ZMAC involves the crucial use of sorption isotherm techniques. Theoretical MO sorption amounts (milligrams per gram) were determined using model equations (Table 3) to identify the most suitable model. Langmuir model demonstrated a great fit to the experimental data, with a correlation coefficient of 0.999, as shown in Figure 7A. This suggests that MO species were effectively covered in a monolayer on the surface of ZMAC, indicating a consistent energy process. ZMAC's Langmuir constant, of the silanol group on the SiO_2 of ZMAC, was determined to be 1.01 L/mg. This finding underscores the positive impact of incorporating carbonaceous materials on the MO species' access to ZMAC adsorption sites.

In contrast, the Freundlich model was not ideal for the MO sorption onto ZMAC, rejecting the hypothesis of a heterogeneous surface, as shown in Figure 7B. Various publications have supported the use of the Langmuir model for MO removal with materials such as activated orange peel powder, CNTs, and Amberlite IRA-420 anion exchangers, as well as AN/CNTs and activated orange peel powder.

Moreover, the Temkin model, in the most recent work, was employed to investigate the heat of adsorption and accurately describe the MO sorption process. Using ZMAC, this model revealed a progressive increase in the adsorption heat in relation to the surface area (Figure 7C). The Temkin isotherm model assumes that the adsorption heat of all molecules decreases linearly with the increase in coverage of the adsorbent surface, and that adsorption is characterized by a uniform distribution of binding energies, up to a maximum binding energy.[48] The observed deviation is characterized by a

https://doi.org/10.1021/acsomega.3c09494
ACS Omega 2024, 9, 13086−13099

Table 4. Sorption Kinetic Parameters for MO Removal Using ZMAC

adsorbent	parameters	ZMAC
pseudo-first order (Lagergren constants)	K_1 (min^{-1})	0.38
	Q_e (mg g^{-1})	22.4
	R^2	0.85
pseudo-second order (Ho and McKay constants)	K_1 (min^{-1})	0.00024
	Q_e (mg g^{-1})	67.5
	R^2	0.956
Elovich constants	β (mg g^{-1} min^{-1})	0.074
	α (mg g^{-1} min^{-1})	3.01
	R^2	0.931
intraparticle constant	C	1.749
	KP	3.7142
	R^2	0.98

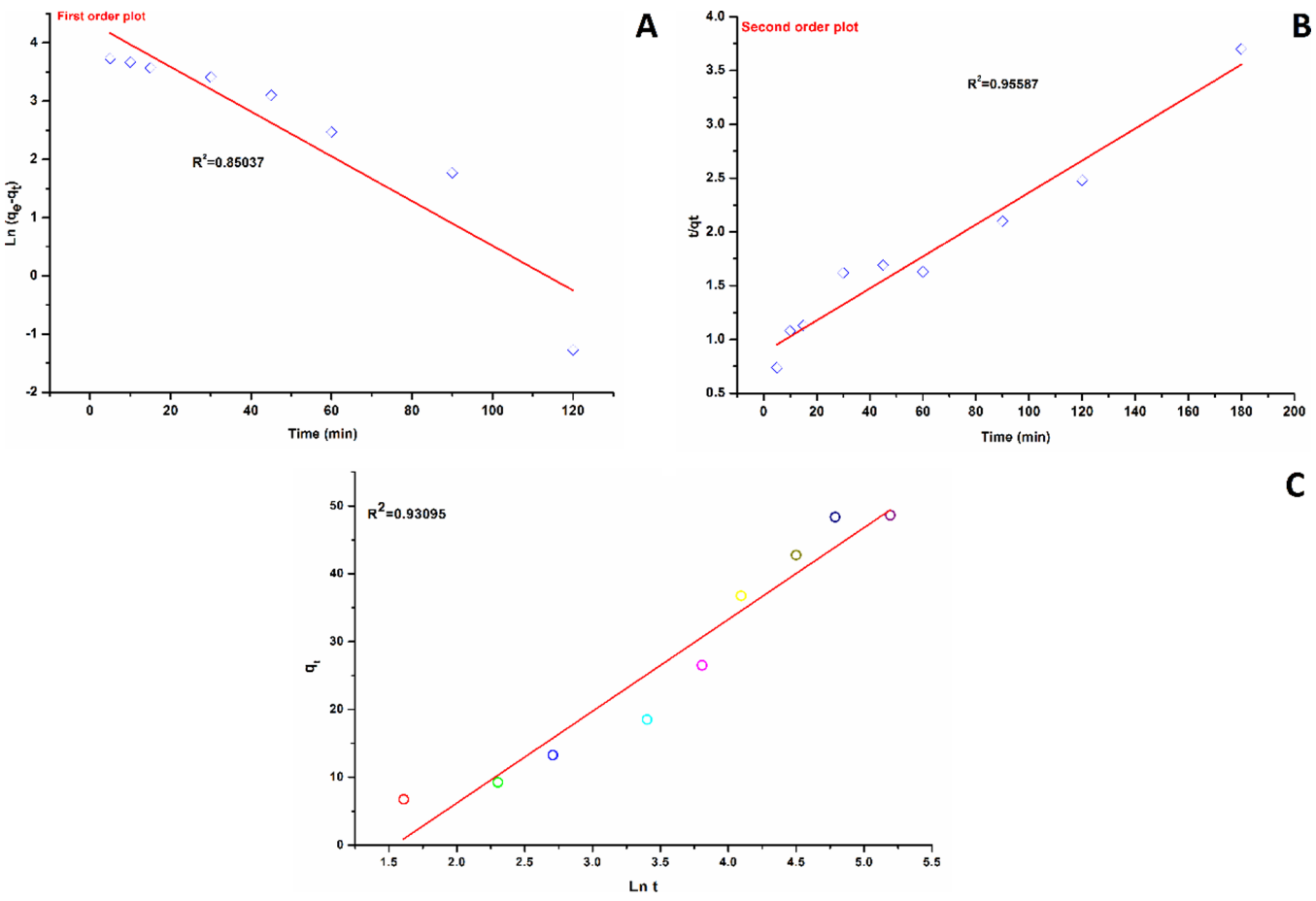

Figure 8. (a) Lagergren, (b) Ho and McKay, and (c) Elovich plots of MO onto ZMAC.

progressive escalation in adsorption heat as the surface area of the ZMAC increases. This departure from the anticipated linear decrease implies a more intricate adsorption process, possibly influenced by factors specific to the ZMAC material. The Temkin model's ability to capture and elucidate this nuanced relationship underscores its effectiveness in describing the thermodynamics of MO sorption onto ZMAC.

Compared to An with CNTs (416.7 mg/g) and Amberlite IRA-420 anion exchanger (20.54 mg/g), the estimated sorption capacity of MO with ZMAC was determined to be 66.2 mg/g,[46,49] with 69.40 mg/g for SiO_2 NPs,[23] 97.1 mg/g or fabricated Fe-loaded chitosan (Fe-CS),[24] 42.85 mg/g for functionalized CNTs-loaded TiO_2,[25] 62.50 mg/g for coffee waste/methylpyridinium chloride,[26] 58.82 mg/g for coffee waste/cetyltrimethylammonium ammonium bromide,[26] and 47.62 mg/g for surfactant-modified pineapple leaf.[27]

3.5. Adsorption Kinetics. Utilizing the linear form of three widely employed kinetic models, we systematically investigated the kinetics of MO removal by ZMAC, including several diffusion models. The kinetics of the sorption process were analyzed using the Lagergren, Ho, McKay, and Elovich equations, as indicated in Table 4. The validity of the equations and the reliance on first-order rate kinetics are demonstrated in Figure 8A, where a straight line is plotted depicting log ($q_e - q$) against time, and pseudo-second-order parameters are demonstrated in Figure 8B. The Elovich

https://doi.org/10.1021/acsomega.3c09494
ACS Omega 2024, 9, 13086−13099

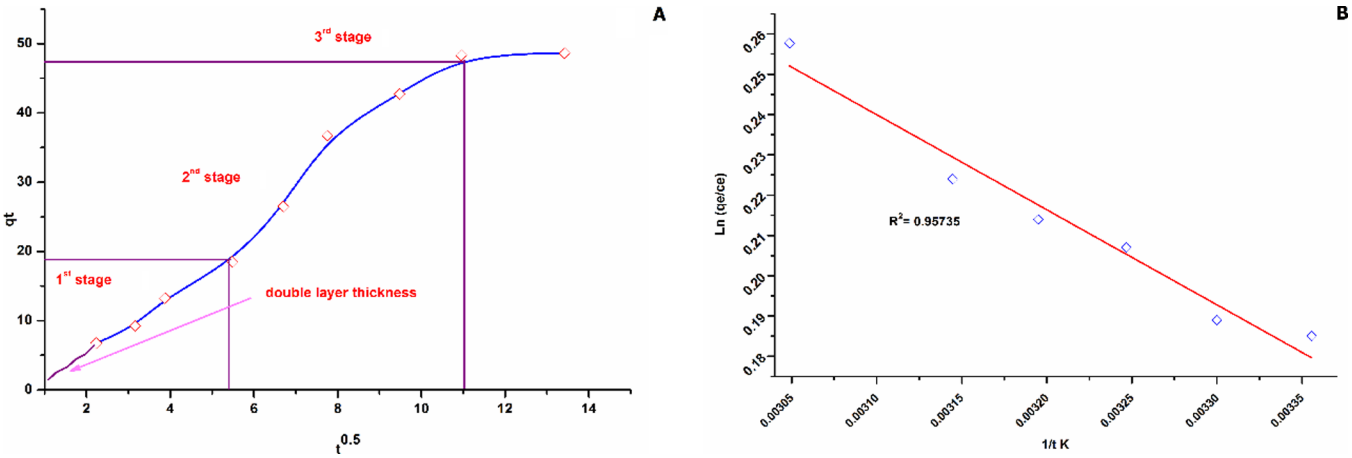

Figure 9. Weber and Morris (A) and Van't Hoff plot (B) versus adsorption process.

equation, which is shown in Figure 8C, can be used to explain adsorption behavior that is identical with the characteristics of chemical adsorption. The relevant results are summarized in Table 4. The associated parameters for MO adsorption onto ZMAC are presented in Table 4.

The regression results for the adsorption of R^2 by the pseudo-first-order, pseudo-second-order, and Elovich equations are displayed in Figure 8A–C and Table 4, respectively. The correlation coefficients fall between 0.85, 0.956, and 0.931, respectively. This also shows that, in contrast to the other two models, the pseudo-second-order equation is the most appropriate for this kind of application.

3.6. Diffusion Rate Constant. MO adsorption process onto ZMAC can be divided into three consecutive stages. (1) External diffusion: this stage involves the molecular diffusion of MO ions to the outer surface of the ZMAC. (2) Internal diffusion: ZMAC acts as a transitional phase, facilitating the movement of MO from the external surface to internal locations within its structure. (3) Intraparticle adsorption: in this final stage, MO particles are adsorbed onto the interior surfaces of the pores and active sites within ZMAC. Assessing the change in the MO concentration over time as it interacts with ZMAC is a common approach for determining the adsorption process rate. The linear relationship is shown in Figure 9. The graph displays three distinct stages: an initial curved portion, then a linear segment, and a plateau stage. The initial curve is attributed to the effects of boundary layer diffusion, while the plateau represents the equilibrium state. The linear segment reflects the intraparticle diffusion processes. Extrapolating from the second stage of the graph back to the time axis at 12° produces intercepts, which can be employed to determine the thickness of the boundary layer. An increase in the intercept size corresponds to a thicker boundary layer.[50]

3.7. Thermodynamic Constants. The impact of temperature (expressed in Kelvin, K) on the adsorption of MO by ZMAC was systematically examined at different temperature levels, specifically 298, 305, 308, 313, and 318 K (Figure 9B). The data presented in Figure 9B illustrate that elevating the temperature from 298 to 318 K resulted in an increase in the uptake capacity, rising from 66.2 to 73.2 mg/g. This temperature effect can be explained by the fact that higher temperatures provide MO ions and ZMAC particles with greater kinetic energy, thus enhancing the likelihood of their mutual attachment. Consequently, MO adsorption onto ZMAC is characterized as an endothermic process. Furthermore, it is well-established that the sorptive forces exerted by the active sites of ZMAC toward MO species can be reinforced with increasing temperature, contributing to augmented MO adsorption. This strengthening of the sorptive forces also extends to the interactions among neighboring MO groups in the adsorbed state.

The thermodynamic parameters, as presented in Table 5, provide additional insights into the adsorption of MO onto ZMAC. Gibbs free energy (ΔG), ranging from −4366 to −4447 J/mol, supports the spontaneous adsorption. Enthalpy (ΔH) and entropy (ΔS) were −1960 kJ/mol and 8.076 J/(mol K), respectively. This indicates an exothermic process, and higher temperatures favor adsorption. Notably, the magnitude of ΔH (−1960 J/mol) is lower than that typically associated with chemisorption, suggesting that the adsorption observed in this case is predominantly physisorption. This implies that the fundamental interaction between MO and ZMAC is likely to overcome most electrostatic interactions.[51]

Table 5. Van't Hoff Plot Corresponding to the Adsorption Process

parameter	ΔH (kJ/mol)	ΔS (J/mol K)	ΔG (kJ/mol)
value	−1.96	8.076	(−4.366) to (−4.447)

The relatively smaller positive value of the entropy change (ΔS) further indicates that there was a lack of randomness at the material interface during the adsorption of the MO onto ZMAC in aqueous solution. This suggests a more ordered and controlled adsorption process.

To further elucidate the nature of the adsorption process, we can employ the Arrhenius equation (eq 10) to access the activation energy (E_a) for adsorption. This activation energy provides insights into whether the process is of a physical or chemical nature. Specifically, when E_a is less than 40 kJ mol^{-1}, it signifies physicosorption, indicating that adsorption primarily involves physical forces. Conversely, when E_a exceeds 40 kJ mol^{-1}, it suggests chemisorption, indicating the presence of a strong chemical bond.

Understanding the nature of adsorption is crucial, as it can provide insights into the underlying mechanisms and help in tailoring adsorption processes for specific applications. In this context, the smaller positive ΔS and the value of E_a can serve as

https://doi.org/10.1021/acsomega.3c09494
ACS Omega 2024, 9, 13086−13099

Table 6. Physicochemical Analysis of Certain Real Industrial Wastewater Sample

items	unit	results before adsorption with ZMAC	results after adsorption with ZMAC	R%
pH	unitless	7.8	7.5	
TDS	mg/L	780	776	
conductivity	μs/cm	1510	1501	
MO	mg/L	40.7	1.22	97
MB	mg/L	23.5	4.7	80
crystal violet	mg/L	18.7	5.423	71

diagnostic tools to differentiate between physicosorption and chemisorption in the MO-ZMAC system.[46]

Adsorption kinetics are employed for the determination of specific parameters, which include the factor A (Arrhenius factor), the rate constant kexp (representing the kinetic adsorption of MO on ZMAC), and the activation energy Ea. The calculated activation energy Ea, which amounts to 15.9 KJ, indicates that this is an exothermic physicochemical sorption process. This implies that heat is released during the adsorption, and the process involves a combination of physical and chemical interactions between MO and ZMAC.

3.8. Comparative Study for Different Dyes Removal Using ZMAC. The physicochemical parameters of the real industrial wastewater sample were recorded before and after treatment with 10 mg of ZMAC agitation time of 3 h, agitation speed of 200 rpm, and a sorbent mass of 10 mg, pH 4, and temperature 20 °C. As shown in Table 6, the level of TDS, conductivity, pH, and dye concentration were determined; no variation of TDS, conductivity, and pH results, due to adsorption process concerned with removal of rare concentration of azo dyes. The removal percentages of MO, MB, and crystal violet are 97, 80, and 71%, respectively.

3.9. Adsorbent Reusability. The capacity of sorbent materials to undergo multiple regeneration cycles is of paramount economic importance due to its influence on production costs. In the context of this study, regenerating the composite that had adsorbed arsenic facilitated restoration of the immediate affinity between the MO and the adsorbent surface. As depicted in Figure 10, the ZMAC composite adsorbent displayed a sustained high affinity, maintaining efficient MO removal (percentage) above 70% even after four consecutive regeneration cycles. These findings underscore the efficacy and recyclability of the synthetic composite as a MO adsorbent, emphasizing its economic viability for repeated use.

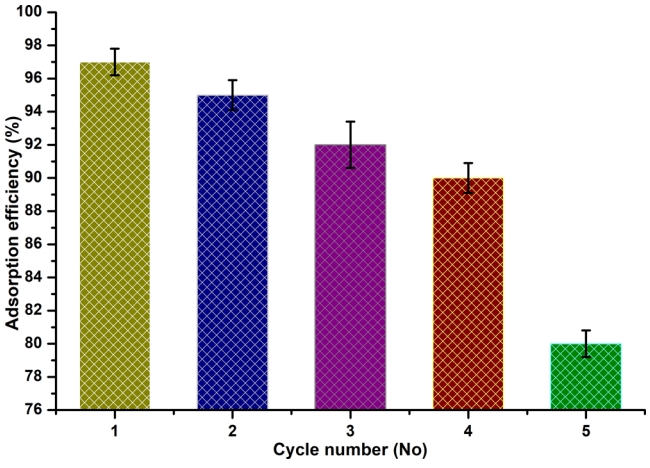

Figure 10. Reusability of the ZMAC adsorbent composite.

3.10. Possible Working Mechanism. Per previous investigations,[47,49] the assessment of the adsorption process can be approached through a comprehensive examination of ZMAC characterization, isothermal testing, and kinetic tests, as depicted in Figure 11. The formation of an electric double

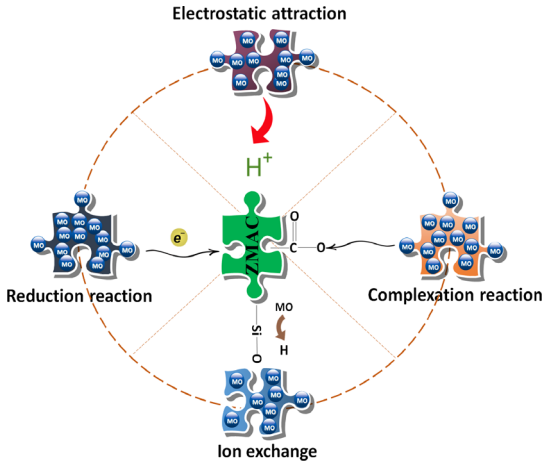

Figure 11. Different mechanisms of interaction between ZMAC and MO.

layer around the MO ions and ZMAC surfaces is attributed to electrostatic interactions. As per the diffuse double layer theory, elevating the ionic strength of the solution causes the double-layer thickness to contract. This contraction enables a closer proximity between the metal ions and carbon atoms. Consequently, attractive forces like van der Waals' forces become more influential, resulting in increased absorption of metal ions.[52]

A chemical exchange transpires at the silica surface, involving a hydrogen bond formed between surface oxygen and the hydrogen atom of the MO. This exchange involves protons from the surface silanol groups swapping places with metal ions from the solution. This process is indicative of a cation-exchange mechanism due to the substantial presence of silica in the sorbent, exceeding 6%[47]

$$\mathrm{MO} + x(\equiv\equiv\mathrm{SiOH}) \leftrightarrow \mathrm{MO}(\equiv\equiv\mathrm{SiO})_x^{(n-x)+} + x\mathrm{OH}^- \quad (13)$$

The silanol group on SiO_2 is indicated by SiOH, and the amount of released hydroxyls is represented by the notation (XOH−).

The adsorption mechanism was defined by the electrostatic pull between the positively charged surfaces of the adsorbent and the negative MO. This observation suggests the involvement of electrostatic forces in the adsorption phenomenon. Because of the protonation of ZMAC exterior surface at pH = 3−5, multiple attractive forces come into play between MO species and the functionalized groups of ZMAC

https://doi.org/10.1021/acsomega.3c09494
ACS Omega 2024, 9, 13086−13099

including electrostatic attraction between MO species and the protonated Si−OH^+ groups of the ZMAC adsorbent.

The nature of the molecule itself is the most significant factor dictating the mechanism of MO adsorption and thereafter the composition of the adsorbent material. The actual physicochemical mechanisms governing the adsorptive absorption can be better understood by studying the chemical properties of the adsorbent and adsorbate.[53] MO is a polycyclic aromatic molecule, and it can interact with adsorbents that have varying degrees of aromaticity through electron donor−acceptor (EDA) interactions. Among the most prominent physical forces influencing MO uptake are these ones. In such a way, adsorptive materials such as ZMAC can interact significantly with MO. MO's hetero atoms on its structure allow it to interact with adsorbents through hydrogen bonding. The appropriate places for weak interactions with hydrogen species on adsorbents are the sodium-substituted sulfur atom on one end and the dimethyl-substituted nitrogen atom on the other. MO can generate strong electrostatic contact with adsorbents that are not at their isoelectric point, since it is an ionizable molecule with a pK_a of 3.4. Strong chemical interactions called electrostatic interactions can be responsible for a large portion of MO absorption in adsorptive systems.[54]

4. CONCLUSIONS

Here, we have systematically investigated the adsorption capabilities of ZMAC as an effective adsorbent for cleaning aqueous solutions from MO. Our findings reveal that ZMAC exhibits remarkable adsorption efficiency, supported by its low pore volume and significant surface area. Optimal conditions for MO adsorption were identified, with the most favorable results obtained under specific settings, such as an agitation time of 3 h, agitation speed of 200 rpm, a sorbent mass of 10 mg, pH 4, and MO concentration of 10 mg/L. The monolayer coverage of MO on ZMAC was determined to be 66.2 mg/g, indicating its high adsorption capacity. Our experimental data closely adhered to the pseudo-second-order kinetics and the Langmuir isotherm models, emphasizing the robustness of ZMAC as an adsorbent for MO removal. Furthermore, the thermodynamic parameters, including the ΔG values, confirm this spontaneous yet efficient adsorption. ΔH and ΔS suggest an exothermic adsorption reaction. Additionally, our study demonstrated the recyclability of ZMAC as an adsorbent, with consistent adsorption percentages observed over multiple regeneration cycles. The regeneration process, involving the use of HNO_3 (2M), maintained the adsorbent's efficacy for at least five cycles. In summary, our research highlights the excellent potential of ZMAC, and its demonstrated adsorption capabilities, coupled with its recyclability, position ZMAC as a promising alternative for MO adsorption, contributing to water treatment. This study underscores the significance of ZMAC as a valuable tool for addressing water pollution challenges and offers insights into its practical application.

AUTHOR INFORMATION

Corresponding Authors

Mohamed R. El-Aassar − *Chemistry Department, College of Science, Jouf University, Sakaka 2014, Saudi Arabia;* orcid.org/0000-0002-9154-6089; Email: mrelaassar@ju.edu.sa

Kawthar A. Omran − *Department of Chemistry, College of Science and Humanities, Shaqra University, Shaqraa 11911, Saudi Arabia; Freshwater & Lakes Division, National Institute of Oceanography Fisheries (NIOF), Cairo 4262110, Egypt*; Email: Kabdeltawab@su.edu.sa

Authors

Fathy M. Mohamed − *Hydrogeology and Environment Department, Faculty of Earth Sciences, Beni-Suef University, Beni-Suef 62521, Egypt*

Omar M. Ibrahim − *Department of Medicine, Washington University School of Medicine, St. Louis, Missouri 63110, United States;* orcid.org/0000-0002-9903-6657

Aya Elsayed − *Hydrogeology and Environment Department, Faculty of Earth Sciences, Beni-Suef University, Beni-Suef 62521, Egypt*

Manal F. Alrakshy − *Faculty of Science, Alasmarya Islamic University, Zliten 495-471, Libya*

Mohamed Abdel Rafea − *Department of Physics, College of Science, Imam Mohammad Ibn Saud Islamic University (IMSIU), Riyadh 11623, Saudi Arabia*

Complete contact information is available at: https://pubs.acs.org/10.1021/acsomega.3c09494

Author Contributions

M.R.E.A. and F.M.M.: funding, conceptualization, methodology, writing—original draft, and writing—review and editing. O.I. and M.F.A.: data curation, formal analysis, writing—original draft, and writing—review and editing. A.N.A. and M.A.R.: methodology, data curation, and formal analysis. K.A.O.: funding, formal analysis, original draft, and writing—review and editing. F.M.M. and O.M.I.: equal contribution as first authors.

Funding

This work was funded by the Science and Technology Development Fund (STDF) under Grant Number (46896), and the authors would like to thank the Deanship of Scientific Research at Shaqra University for supporting this work.

Notes

The authors declare no competing financial interest.

ACKNOWLEDGMENTS

The authors thank Science and Technology Development Fund (STDF) for funding this project. The authors would like to thank the Deanship of Scientific Research at Shaqra University for supporting this work.

REFERENCES

(1) Zhao, L.; Yang, F.; Jiang, Q.; Zhu, M.; Jiang, Z.; Tang, Y.; Zhang, Y. Characterization of Modified Biochars Prepared at Low Pyrolysis Temperature as an Efficient Adsorbent for Atrazine Removal. *Environmental Science and Pollution Research* **2018**, *25* (2), 1405−1417.

(2) Samsudin, E. M.; Goh, S. N.; Wu, T. Y.; Ling, T. T.; Hamid, S. B. A.; Juan, J. C. Evaluation on the photocatalytic degradation activity of reactive blue 4 using pure anatase nano-TiO_2. *Sains Malays.* **2015**, *44* (7), 1011−1019.

(3) Hussein, F. H. Effect of Photocatalytic Treatments on Physical and Biological Properties of Textile Dyeing Wastewater. *Asian J. Chem.* **2013**, *25* (16), 9387−9392, DOI: 10.14233/ajchem.2013.15909.

(4) Khamis Soliman, N.; Moustafa, A. F.; Aboud, A. A.; Halim, K. S. A. Effective utilization of Moringa seeds waste as a new green environmental adsorbent for removal of industrial toxic dyes. *J. Mater. Res. Technol.* **2019**, *8* (2), 1798−1808.

https://doi.org/10.1021/acsomega.3c09494
ACS Omega 2024, 9, 13086−13099

(5) Balarak, D.; Mahdavi, Y.; Bazrafshan, E.; Mahvi, A. H. Kinetic, isotherms and thermodynamic modeling for adsorption of Acid Blue 92 (AB92) from aqueous solution by modified Azolla filicoloides. *Fresenius Environ. Bull.* **2016**, *25* (5), 1322−1331.
(6) Guo, J.; Qiu, L.; Deng, Z.; Yan, F. Plastic reusable pH indicator strips: preparation via anion-exchange of poly (ionic liquids) with anionic dyes. *Polym. Chem.* **2013**, *4* (5), 1309−1312.
(7) Iwuozor, K. O.; Ighalo, J. O.; Emenike, E. C.; Ogunfowora, L. A.; Igwegbe, C. A. Adsorption of methyl orange: A review on adsorbent performance. *Current Research in Green and Sustainable Chemistry* **2021**, *4*, No. 100179.
(8) Demir, M.; Kahveci, Z.; Aksoy, B.; Palapati, N. K. R.; Subramanian, A.; Cullinan, H. T.; El-Kaderi, H. M.; Harris, C. T.; Gupta, R. B. Graphitic Biocarbon from Metal-Catalyzed Hydrothermal Carbonization of Lignin. *Ind. Eng. Chem. Res.* **2015**, *54* (43), 10731−10739.
(9) Owolabi, A. F.; Haafiz, M. K. M.; Hossain, M. S.; Hussin, M. H.; Fazita, M. R. N. Influence of Alkaline Hydrogen Peroxide Pre-Hydrolysis on the Isolation of Microcrystalline Cellulose from Oil Palm Fronds. *Int. J. Biol. Macromol.* **2017**, *95*, 1228−1234.
(10) Uzma, N. Adsorption of Pb (II) from Aqueous Solutions by Activated Carbon Prepared from Agricultural Waste: Maize Leaves. *Eur. Chem. Bull.* **2013**, *2* (11), 927−931.
(11) Reza, R. A.; Ahmaruzzaman, M. A Novel Synthesis of Fe_2O_3@ Activated Carbon Composite and Its Exploitation for the Elimination of Carcinogenic Textile Dye from an Aqueous Phase. *Rsc Advances* **2015**, *5* (14), 10575−10586.
(12) Lin, S.-H.; Juang, R.-S. Adsorption of Phenol and Its Derivatives from Water Using Synthetic Resins and Low-Cost Natural Adsorbents: A Review. *Journal of environmental management* **2009**, *90* (3), 1336−1349.
(13) Querejeta, N.; Plaza, M. G.; Rubiera, F.; Pevida, C. Water Vapor Adsorption on Biomass Based Carbons under Post-Combustion CO2 Capture Conditions: Effect of Post-Treatment. *Materials* **2016**, *9* (5), 359.
(14) Elzain, A. A.; El-Aassar, M. R.; Hashem, F. S.; Mohamed, F. M.; Ali, A. S. M. Removal of Methylene Dye Using Composites of Poly (Styrene-Co-Acrylonitrile) Nanofibers Impregnated with Adsorbent Materials. *J. Mol. Liq.* **2019**, *291*, No. 111335, DOI: 10.1016/j.molliq.2019.111335.
(15) Wu, Y.; Guo, J.; Han, Y.; Zhu, J.; Zhou, L.; Lan, Y. Insights into the Mechanism of Persulfate Activated by Rice Straw Biochar for the Degradation of Aniline. *Chemosphere* **2018**, *200*, 373−379.
(16) Oleszczuk, P.; Godlewska, P.; Reible, D. D.; Kraska, P. Bioaccessibility of Polycyclic Aromatic Hydrocarbons in Activated Carbon or Biochar Amended Vegetated (Salix Viminalis) Soil. *Environ. Pollut.* **2017**, *227*, 406−413.
(17) Yan, B.; Niu, C. H.; Wang, J. Kinetics, Electron-Donor-Acceptor Interactions, and Site Energy Distribution Analyses of Norfloxacin Adsorption on Pretreated Barley Straw. *Chemical engineering journal* **2017**, *330*, 1211−1221.
(18) Sarvani, R.; Damani, E.; Ahmadi, S. Adsorption Isotherm and Kinetics Study: Removal of Phenol Using Adsorption onto Modified Pistacia Mutica Shells. *Iran. J. Health Sci.* **2018**, *6*, 33−42.
(19) El Gamala, M.; Mohamedb, F. M.; Mekewic, M. A.; Hashemc, F. S.; El-Aassard, M. R.; Khalifae, R. E. Adsorptive Removal of Methyl Orange from Aqueous Solutions by Polyvinylidene Fluoride Tri-Flouro Ethylene/Carbon Nanotube/Kaolin Nanocomposite: Kinetics, Isotherm, and Thermodynamics. *Desalin. Water Treat.* **2020**, *193*, 142−151.
(20) Mengmeng, Z.; Xiongmu, C.; Lingxiao, L. I. Preparation and Characterization of Micro/Mesoporous Activated Carbon from Denitrided Residue of Waste Penicillin Mycelium. *Chem. Ind. Eng. Progr.* **2018**, *37* (12), 4773−4781.
(21) Zhao, W.; Cao, L.; Huang, X. Microwave Prepared Straw Activated Carbon and Its Impact on Toluene Adsorption. *Environ. Sci. Technol.* **2014**, *37* (10), 108−116.
(22) Han, R.; Fang, Y.; Sun, P.; Xie, K.; Zhai, Z.; Liu, H.; Liu, H. N-Doped Biochar as a New Metal-Free Activator of Peroxymonosulfate for Singlet Oxygen-Dominated Catalytic Degradation of Acid Orange 7. *Nanomaterials* **2021**, *11* (9), 2288.
(23) Zhang, X.; Saravanakumar, K.; Sathiyaseelan, A.; Lu, Y.; Wang, M. H. Adsorption of methyl orange dye by SiO2 mesoporous nanoparticles: adsorption kinetics and eco-toxicity assessment in Zea mays sprout and Artemia salina. *Environ. Sci. Pollut. Res.* **2023**, *30*, 117000−117010.
(24) Abdul Mubarak, N. S.; Chuan, T. W.; Khor, H. P.; Jawad, A. H.; Wilson, L. D.; Sabar, S. Immobilized Fe-loaded chitosan film for methyl orange dye removal: competitive ions, reusability, and mechanism. *Journal of Polymers and the Environment* **2021**, *29*, 1050−1062.
(25) Ahmad, A.; Razali, M. H.; Mamat, M.; Mehamod, F. S. B.; Amin, K. A. M. Adsorption of methyl orange by synthesized and functionalized-CNTs with 3-aminopropyltriethoxysilane loaded TiO_2 nanocomposites. *Chemosphere* **2017**, *168*, 474−482.
(26) Iwuozor, K. O.; Ighalo, J. O.; Emenike, E. C.; Ogunfowora, L. A.; Igwegbe, C. A. Adsorption of methyl orange: A review on adsorbent performance. *Current Research in Green and Sustainable Chemistry* **2021**, *4*, No. 100179.
(27) Kamaru, A. A.; Sani, N. S.; Malek, N. A. N. N. Raw and surfactant-modified pineapple leaf as adsorbent for removal of methylene blue and methyl orange from aqueous solution. *Desalination and Water Treatment* **2016**, *57* (40), 18836−18850.
(28) Water Environment Federation; American Water Works Association. *Standard Methods for the Examination of Water and Wastewater*; American Public Health Association (APHA): Washington, DC, USA, 2005, p. 21.
(29) El-Aassar, M. R.; Mohamed, F. M.; Alsohaimi, I. H.; Khalifa, R. E. Fabrication of Novel Valorized Ecofriendly Olive Seed Residue/Anthracite/Chitosan Composite for Removal of Cr (VI): Kinetics Isotherms and Thermodynamics Modeling. *Cellulose* **2021**, *28* (11), 7165−7183.
(30) El-Aassar, M. R.; Masoud, M. S.; Elkady, M. F.; Elzain, A. A. Synthesis, Optimization, and Characterization of Poly (Styrene-co-Acrylonitrile) Copolymer Prepared via Precipitation Polymerization. *Advances in Polymer Technology* **2018**, *37* (6), 2021−2029.
(31) El-Aassar, M. R.; Mohamed, F. M. Characterization Valorized Anthracite and Its Application in Manganese (VII) Adsorption from Aqueous Solution; Batch and Column Studies. *Microporous Mesoporous Mater.* **2021**, *310*, No. 110641.
(32) Khalifa, R. E.; Omer, A. M.; Tamer, T. M.; Ali, A. A.; Ammar, Y. A.; Eldin, M. S. M. Efficient Eco-Friendly Crude Oil Adsorptive Chitosan Derivatives: Kinetics, Equilibrium and Thermodynamic Studies. *Desalin. Water Treat.* **2019**, *159*, 269−281.
(33) Langmuir, I. The Constitution and Fundamental Properties of Solids and Liquids II. Liquids. *Journal of the American chemical society* **1917**, *39* (9), 1848−1906.
(34) Freundlich, H. Über Die Adsorption in Lösungen. *Z. Phys. Chem.* **1907**, *57* (1), 385−470.
(35) Tempkin, M. I.; Pyzhev, V. Kinetics of Ammonia Synthesis on Promoted Iron Catalyst. *Acta Phys. Chim. USSR* **1940**, *12* (1), 327.
(36) Lagergren, S. K. About the Theory of So-Called Adsorption of Soluble Substances. *Sven. Vetenskapsakad. Handingarl* **1898**, *24*, 1−39.
(37) Ho, Y.-S.; McKay, G. Pseudo-Second Order Model for Sorption Processes. *Process biochemistry* **1999**, *34* (5), 451−465.
(38) Omer, A. M.; Elgarhy, G. S.; El-Subruiti, G. M.; Khalifa, R. E.; Eltaweil, A. S. Fabrication of Novel Iminodiacetic Acid-Functionalized Carboxymethyl Cellulose Microbeads for Efficient Removal of Cationic Crystal Violet Dye from Aqueous Solutions. *Int. J. Biol. Macromol.* **2020**, *148*, 1072−1083.
(39) Byamba-Ochir, N.; Shim, W. G.; Balathanigaimani, M. S.; Moon, H. Highly Porous Activated Carbons Prepared from Carbon Rich Mongolian Anthracite by Direct NaOH Activation. *Appl. Surf. Sci.* **2016**, *379*, 331−337.
(40) Eckmann, A.; Felten, A.; Mishchenko, A.; Britnell, L.; Krupke, R.; Novoselov, K. S.; Casiraghi, C. Probing the Nature of Defects in Graphene by Raman Spectroscopy. *Nano Lett.* **2012**, *12* (8), 3925−3930.

https://doi.org/10.1021/acsomega.3c09494
ACS Omega 2024, 9, 13086−13099

(41) Mohan, A. N.; Manoj, B.; Ramya, A. V. Probing the Nature of Defects of Graphene like Nano-Carbon from Amorphous Materials by Raman Spectroscopy. *Asian J. Chem.* **2016**, *28* (7), 1501.
(42) Ramya, K.; John, J.; Manoj, B. Raman Spectroscopy Investigation of Camphor Soot: Spectral Analysis and Structural Information. *Int. J. Electrochem. Sci.* **2013**, *8*, 9421−9428.
(43) Kan, Y.; Yue, Q.; Li, D.; Wu, Y.; Gao, B. Preparation and Characterization of Activated Carbons from Waste Tea by H3PO4 Activation in Different Atmospheres for Oxytetracycline Removal. *Journal of the Taiwan Institute of Chemical Engineers* **2017**, *71*, 494−500.
(44) Gregg, S. J.; Sing, K. S. W.; Salzberg, H. W. Adsorption Surface Area and Porosity. *J. Electrochem. Soc.* **1967**, *114* (11), 279Ca.
(45) Tchuifon, D. R.; Anagho, S. G.; Njanja, E.; Ghogomu, J. N.; Ndifor-Angwafor, N. G.; Kamgaing, T. Equilibrium and kinetic modelling of methyl orange adsorption from aqueous solution using rice husk and egussi peeling. *Int. J. Chem. Sci.* **2014**, *12* (3), 741−761.
(46) Mouraille, N. E. L.; Belmouden, M.; Ichou, Y. A.; *Investigation on Adsorption Capacity of TiO2 in the Removal of A Commercial Pesticide: A Kinetic Study*; 2016.
(47) Mohamed, F. M.; Alfalous, K. A. The Effectiveness of Activated Silica Derived from Rice Husk in Coagulation Process Compared with Inorganic Coagulants for Wastewater Treatment. *Egyptian Journal of Aquatic Research* **2020**, *46* (2), 131−136.
(48) Piccin, J. S.; Dotto, G. L.; Pinto, L. A. A. Adsorption isotherms and thermochemical data of FD&C Red n 40 binding by chitosan. *Brazilian Journal of Chemical Engineering* **2011**, *28*, 295−304.
(49) Eldin, M. S. M.; Alamry, K. A.; Al-Malki, M. A. Kinetic and Isothermal Studies of Manganese (VII) Ions Removal Using Amberlite IRA-420 Anion Exchanger. *Desalin. Water Treat.* **2017**, *72*, 30−40.
(50) Patrick, J. W. *Porosity in Carbons: Characterization and Applications*; Wiley, 1995.
(51) Alkan, M.; Demirbaş, Ö.; Çelikçapa, S.; Doğan, M. Sorption of Acid Red 57 from Aqueous Solution onto Sepiolite. *Journal of hazardous materials* **2004**, *116* (1−2), 135−145.
(52) Abo-El-Enein, S. A.; Eissa, M. A.; Diafullah, A. A.; Rizk, M. A.; Mohamed, F. M. Removal of Some Heavy Metals Ions from Wastewater by Copolymer of Iron and Aluminum Impregnated with Active Silica Derived from Rice Husk Ash. *Journal of Hazardous Materials* **2009**, *172* (2−3), 574−579.
(53) Igwegbe, C. A.; Aniagor, C. O.; Oba, S. N.; Yap, P. S.; Iwuchukwu, F. U.; Liu, T.; de Souza, E. C.; Ighalo, J. O. Environmental protection by the adsorptive elimination of acetaminophen from water: A comprehensive review. *Journal of Industrial and Engineering Chemistry* **2021**, *104*, 117−135.
(54) Cavali, M.; Junior, N. L.; de Sena, J. D.; Woiciechowski, A. L.; Soccol, C. R.; Belli Filho, P.; Bayard, R.; Benbelkacem, H.; de Castilhos Junior, A. B. A review on hydrothermal carbonization of potential biomass wastes, characterization and environmental applications of hydrochar, and biorefinery perspectives of the process. *Sci. Total Environ.* **2023**, *857*, No. 159627.

https://doi.org/10.1021/acsomega.3c09494
ACS Omega 2024, 9, 13086−13099